



LIGO Laboratory / LIGO Scientific Collaboration

LIGO- T060267-00-D

1/04/06

Upgrading the Input Optics for High Power Operation

UF LIGO Group, IAP Group

Distribution of this document:
LIGO Science Collaboration

This is an internal working note
of the LIGO Project.

California Institute of Technology
LIGO Project – MS 18-34
1200 E. California Blvd.
Pasadena, CA 91125
Phone (626) 395-2129
Fax (626) 304-9834
E-mail: info@ligo.caltech.edu

Massachusetts Institute of Technology
LIGO Project – NW17-161
175 Albany St
Cambridge, MA 02139
Phone (617) 253-4824
Fax (617) 253-7014
E-mail: info@ligo.mit.edu

LIGO Hanford Observatory
P.O. Box 1970
Mail Stop S9-02
Richland WA 99352
Phone 509-372-8106
Fax 509-372-8137

LIGO Livingston Observatory
P.O. Box 940
Livingston, LA 70754
Phone 225-686-3100
Fax 225-686-7189

<http://www.ligo.caltech.edu/>

Abstract

Sometime during S5 or after its completion, the LIGO detectors will undergo a series of technical improvements designed to increase their sensitivity. Among these improvements, the laser power will be increased to deliver approximately 30 W to the PRM. At these power levels, both the electro-optic modulators (EOMs) and the Faraday isolators (FIs) will need to be replaced. Absorption in the current FIs and subsequent heating will lead to enhanced thermal effects: thermal lensing, thermal birefringence, and beam steering. The current New Focus LiNbO₃ modulators will also suffer from severe thermal lensing.

We propose that the current EOMs be replaced with a UF design for Advanced LIGO based on RTP. These modulators are similar to the current New Focus modulators in electro-optics performance, but the RTP crystal has significantly lower absorption and therefore thermal lensing.

We also propose to replace the FIs with a new design, essentially equivalent to what is proposed for Advanced LIGO. The new FI design minimizes thermal birefringence by using two TGG crystals and a quartz rotator which cancel thermally induced birefringence and DKDP, a $-dn/dt$ material to compensate thermal lensing.

Performance data and implementation issues are discussed in this document.

Acronyms

DKDP – deuterated potassium dihydrogen phosphate

FI – Faraday isolator

FR- Faraday rotator

EOM – Electro-optic modulator

IAP – Institute of Applied Physics

MMT – suspended mode matching telescope mirror

PRM – power recycling mirror

QR – quartz rotator

REFL – symmetric port reflected beam

RTA – Rubidium titanyl arsenate

RTP – Rubidium titanyl phosphate

SM – suspended steering mirror

TFP – thin film polarizers

TGG – terbium gallium garnet

1 Electro-optic modulator

1.1 RF Modulation Requirements

The requirements on optical modulation, including modulation frequencies, modulation depths, and relative stability of the modulation frequency and amplitude¹, for Advanced LIGO are described in the IO DRD, LIGO-T020020. Since these requirements are at least as stringent as those of initial LIGO, we adopt them here.

1.2 Modulator Material's Properties

1.2.1 Optical and Electro-optical Properties

After a literature survey, consultation with Crystal Associates and Raicol Corporation, and experiments in our lab, we have chosen rubidium titanyl phosphate (RbTiOPO₄ or RTP) for the modulator material in advanced LIGO. A related material, rubidium titanyl arsenate (RTA), also meets requirements and we are carrying that as an alternate. The standard modulator material, used in initial LIGO, lithium niobate (LiNbO₃), is not satisfactory from the point of view of thermal lensing, damage, and residual absorption. A summary of the properties of RTP, RTA, and LiNbO₃ is shown in Table 1.

Table 1 - Material Parameters for Selected EOM Crystals^{a)}

Properties	Units/conditions	RTP	RTA	LiNbO ₃
Damage Threshold	MW/cm ² , (10ns, 1064 nm)	>600 (AR coated)	400	280
n_x	1064nm	1.742	1.811	2.23
n_y	1064nm	1.751	1.815	2.23
n_z	1064nm	1.820	1.890	2.16
Absorption coefficient α	cm ⁻¹ (1064 nm)	< 0.0005	< 0.005	< 0.005
r_{33}	pm/V	39.6	40.5	30.8
r_{23}	pm/V	17.1	17.5	8.6
r_{13}	pm/V	12.5	13.5	8.6
r_{42}	pm/V	?	?	28
r_{51}	pm/V	?	?	28
r_{22}	pm/V			3.4

¹ LIGO T020021, "Sideband Requirements in Advanced LIGO, Part I", G. Mueller, et al.

$n_z^3 r_{33}$	pm/V	239	273	306
Dielectric const., ϵ_z	500 kHz, 22 °C	30	19	
Conductivity, σ_z	$\Omega^{-1}\text{cm}^{-1}$, 10 MHz	$\sim 10^{-9}$	3×10^{-7}	
Loss Tangent, d_z	500 kHz, 22 °C	1.18	-	

- a) Data from Raicol, Crystal Associates, Coretech, Note that the reported data are not all consistent. Moreover, many are strongly temperature and frequency dependent, particularly the conductivity and loss tangent..

The largest EO-coefficient is r_{33} . The optimum configuration is propagation direction in the y-direction; applied electrical field and polarization of the light field in the z-direction. The modulation depth is then:

$$\Delta\Phi = m = \frac{\pi L}{\lambda} r_{33} n_z^3 \frac{U_z}{d}$$

where L is the length of the crystal, U_z the voltage across the crystal, and d the thickness in the z -direction. The modulation depth of $m = 0.5$ leads to:

$$U_z \frac{L}{d} = 620V \text{ for RTA} \quad \text{and} \quad = 708V \text{ for RTP.}$$

For typical dimensions, $L = 2.0$ cm and $d = 0.4$ cm, $U_z = 124$ V. A resonant circuit, with the RTP crystal as the capacitor, reduces the required input voltage by the Q of the resonator, typically 5-20.

The low electric conductivity (high resistivity) of RTP reduces the electric power consumption inside the crystal to well below the microwatt range, negligible compared to the heat generated by the resistance of the leads and the electrodes. Moreover, the heat produced by the laser beam itself is more critical because of its nonuniform spatial distribution.

1.2.2 Thermal Properties

The thermal properties of RTP and RTA, measured by several workers, are summarized in Table 2. Thermal lensing scales as the parameter Q :

$$Q \equiv \frac{dn}{dT} \frac{\alpha}{\kappa}$$

Table 2 - Comparison of Thermal Properties of RTP, KTP, and LiNbO₃

Properties	Units	RTP	RTA	KTP	LiNbO ₃
dn_x/dT	$10^{-6}/\text{K}$	-	-	11 ^(b)	5.4 ^(c)
dn_y/dT	$10^{-6}/\text{K}$	2.79 ^(a)	5.66 ^(a)	13 ^(b)	5.4 ^(c)
dn_z/dT	$10^{-6}/\text{K}$	9.24 ^(a)	11.0 ^(a)	16 ^(b)	37.9 ^(c)

κ_x	W/Km	3	(e)	2	5.6 ^(d)
κ_y	W/Km	3	(e)	3	5.6 ^(d)
κ_z	W/Km	3	(e)	3	5.6 ^(d)
α	cm ⁻¹	< 0.0005 ^(e)	< 0.005 ^(e)	< 0.005 ^(e)	< 0.05
Q_x	1/W	-	-	2.2	4.8
Q_y	1/W	0.047	0.94	2.2	4.8
Q_z	1/W	0.15	1.83	2.7	34

- a) "Temperature-dependent dispersion relations for RbTiOPO4 and RbTiOAsO4," I. Yutsis, B. Kirshner, and A. Arie, Appl. Phys. B 79, 77 (2004). The x -axis values were not measured, but should be close to those along the y axis.
- b) Handbook of Optics, no wavelength specified,
- c) Crystal Technology, Inc.
- d) only one value given, no axis specified.
- e) For the KTP, KTA, and RTP absorption coefficients, the largest value is for electric field along z , as that is the direction of highest dc conductivity and RF loss tangent.

1.2.3 Comparison with LiNbO₃

The larger optical absorption in LiNbO₃ makes for much stronger thermal lensing than in RTP or RTA. Moreover, the 7:1 anisotropy in dn/dT results in a large ellipticity in the beam profile as observed in some of our experiments. In addition, surface damage was also occasionally observed at > 30 W powers. *Thus, LiNbO₃ will not suffice as a modulator material for Advanced LIGO. It also will not suffice for use in an upgrade to 30 W.*

1.2.4 RTP

Comparing RTP to LiNbO₃, the ratio of dn/dT to κ for the z -axis in LiNbO₃ and for the worst case in KTP is similar. The smaller absorption coefficient is where the benefit of RTP is found.

The expected thermal lens in the modulator can be estimated from the sag change over the beam profile:²

$$\delta s \approx 0.1 \frac{\alpha L P}{\kappa} \frac{dn}{dT} \approx 0.9 \mu m \frac{\alpha}{[10^{-2} / cm]} \frac{L}{[1.5 cm]} \frac{P}{[200 W]}.$$

² Justin D. Mansell, Joseph Hennawi, Eric Gustafson, Martin Fejer, Robert L. Byer, David Clubley, S. Yoshida, and D. H. Reitze, "Evaluating the effect of transmissive optic thermal lensing on laser beam quality using a Shack-Hartmann wavefront sensor", Appl. Opt. **40**, 366-374 (2001).

This leads to a thermal lens of

$$f \approx \frac{w^2}{\delta s} \approx 1m \left(\frac{w}{[mm]} \right)^2 \left(\frac{[\mu m]}{\delta s} \right).$$

For an absorption coefficient of $\alpha=5 \times 10^{-4} \text{ cm}^{-1}$ and a 1 mm beam waist, the sag change is 50 nm and the focal length of the induced lens would be 20 m. Raicol reports a total absorption coefficient for RTP as low as 50 ppm/cm (including scattering and 2nd harmonic generation), one order of magnitude lower than the absorption coefficient used above. The subsequent sag change in the beam would be about 0.4% of the optical wavelength for 200 W power, the thermally induced lens in the 200 m range, and the higher-order mode content less than a percent.

Note that the absorption coefficients given in Table 1 include also non-thermal losses, such as scattering, 2nd harmonic generation, etc. Therefore, the absorption values are upper limits for the thermal problems we could expect and it is possible that heat producing absorption coefficient will be lower. According to information from a variety of sources, the heat producing absorption coefficient in KTP is much lower than in LiNbO₃.

1.2.5 RTP thermal lensing measurements

We have made a number of studies of thermal lensing in RTP. One example is given in the IO Conceptual Design Document (LIGO T-020022). Fig 1 illustrates the measured beam divergence angle for various input powers up to 60 W. For these measurements, the RTP crystal was located at $z=32 \text{ cm}$, and measurements were taken with a Photon, Inc. Beam Scan. Measurements were also taken with and without the RTP in place to determine the background thermal lensing in other

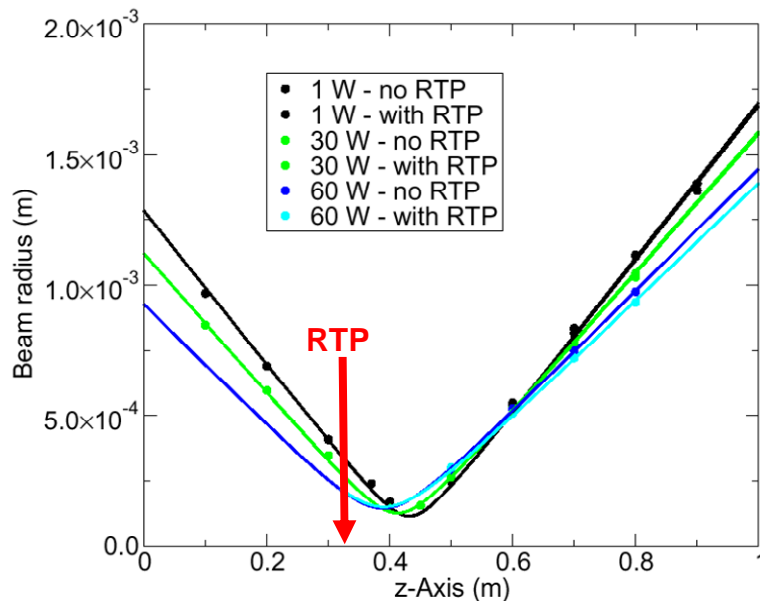


Fig 1 – Measurement of the change in divergence angle as a function of incident laser power. The RTP crystal was located at 32 cm along the Z-axis. Changes were recorded as function of power at 1 W, 30 W, and 60 W with and without the RTP in place.

optical components. The upstream optical components exhibited significant thermal lensing, perhaps due to absorption in the AR coatings, and thus the spot size in the crystal decreased as the power was increased: 700 μm (1 W), 550 μm (30 W), and 450 μm (60 W). A positive thermal lens in the RTP, as expected for $+dn/dT$, would shift the waist closer to the crystal position and increase the divergence angle.

From Fig. 1, we see no difference in the waist position or beam divergence at 1 W and 30 W. At 60 W, a very slight *decrease* is seen in divergence angle, although there is no noticeable shift in the waist position. The measurement error associated with the fitting was greater than the observed change in the beam divergence angle, *thus within the measurement accuracy there is no thermal lensing observable*.

1.3 Modulator Design

We have made RTP-based phase modulators using 1.5 cm long x 0.4 cm width x 0.4 cm thickness crystals. The crystal electrodes were gold over titanium. Clipping losses of a $w = 360 \mu\text{m}$ Gaussian beam radius (roughly the value in the current EOMs) are below 60 ppm.

1.3.1 Mechanical Layout

The modulator is enclosed in an industry-standard housing, nearly identical in details to the modulators used in initial LIGO. The housing, which was manufactured in-house, is shown in Fig. 2. The crystal is on the right hand side of the enclosure, and the impedance matching circuit on the left. There is an SMA connector on the side. The housing is made of aluminum.

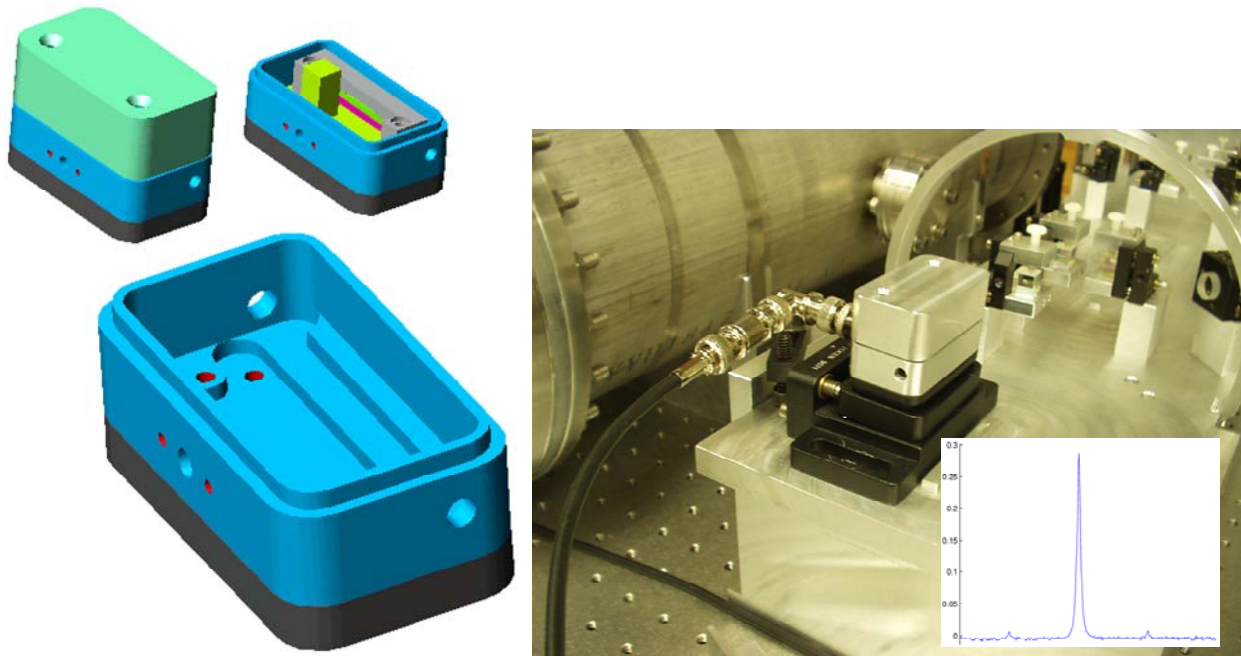


Fig 2 – Housing for the UF-designed electro-optic modulators. It is based on New Focus housing. The connector coming from the housing is an SMA connector.

1.3.2 Impedance matching

Fig. 3. shows the equivalent circuit of the matching network. The matching circuit is designed to have an input impedance of 50Ω and resonantly enhances the RF voltage at the crystal by Q , where Q is the quality factor of the resonator.

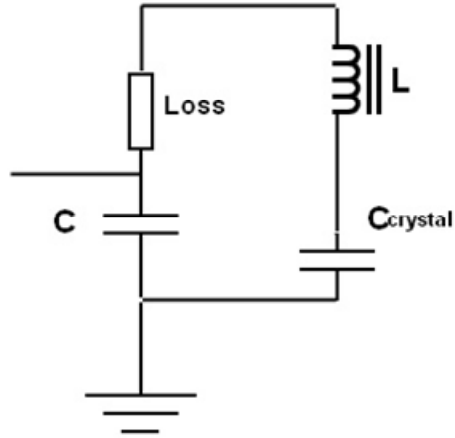


Fig. 3. Equivalent circuit of the matching network.

We have made matching networks for $f = 19.7$ MHz and 180 MHz. The crystal has $C = 6$ pF and the loss (associated with the electrodes and the electrical wiring) is about 2Ω . The shunt capacitance is in the 20 pF range. The 19.7 MHz circuit had $Q = 20$ while the 180 MHz circuit had $Q = 3$.

1.4 Modulator Performance

1.4.1 Low Frequency

The $f = 19.7$ MHz modulator gave a modulation index $m = 0.2$ with 5 V rms drive. Based on this, 12.5 V rms will be required to give $m = 0.5$. The RF generator will need to provide 4 W into 50Ω .

1.4.2 High Frequency

The $f = 180$ MHz modulator gave $m = 0.2$ with 30 V rms drive. Based on this, 75 V rms will be required to give $m = 0.5$. The RF generator would need to provide 120 W into 50Ω for a modulation index of $m = 0.5$.

1.4.3 RFAM Measurements

Pure phase modulated light has a constant intensity. Defects in this are RFAM. RFAM is not objectionable by itself, as the dispersive response of the interferometer and the cavities turn phase modulation into amplitude modulation. However the requirements on fluctuations in the amplitude modulation must meet the requirements discussed in LIGO-T020020.

We have made a number of measurements of the RFAM generated by the RTP modulator. This is a difficult measurement, because the RFAM is near the limit of measurements. Moreover, a power-stabilized, 180 W, single-longitudinal-mode laser is really needed for these measurements.

The best results to date used a pump-probe method with a 40 W heating laser and a 200 mW NPRO probe laser. The RFAM on the probe beam was measured with a calibrated diode using a spectrum analyzer at 19.7 MHz. The dc power of the probe was also measured. The results are shown in Fig. 4. The upper panel shows the ratio of the power in the probe beam at 19.7 MHz to that at dc. The lower panel shows the power from the heating beam.

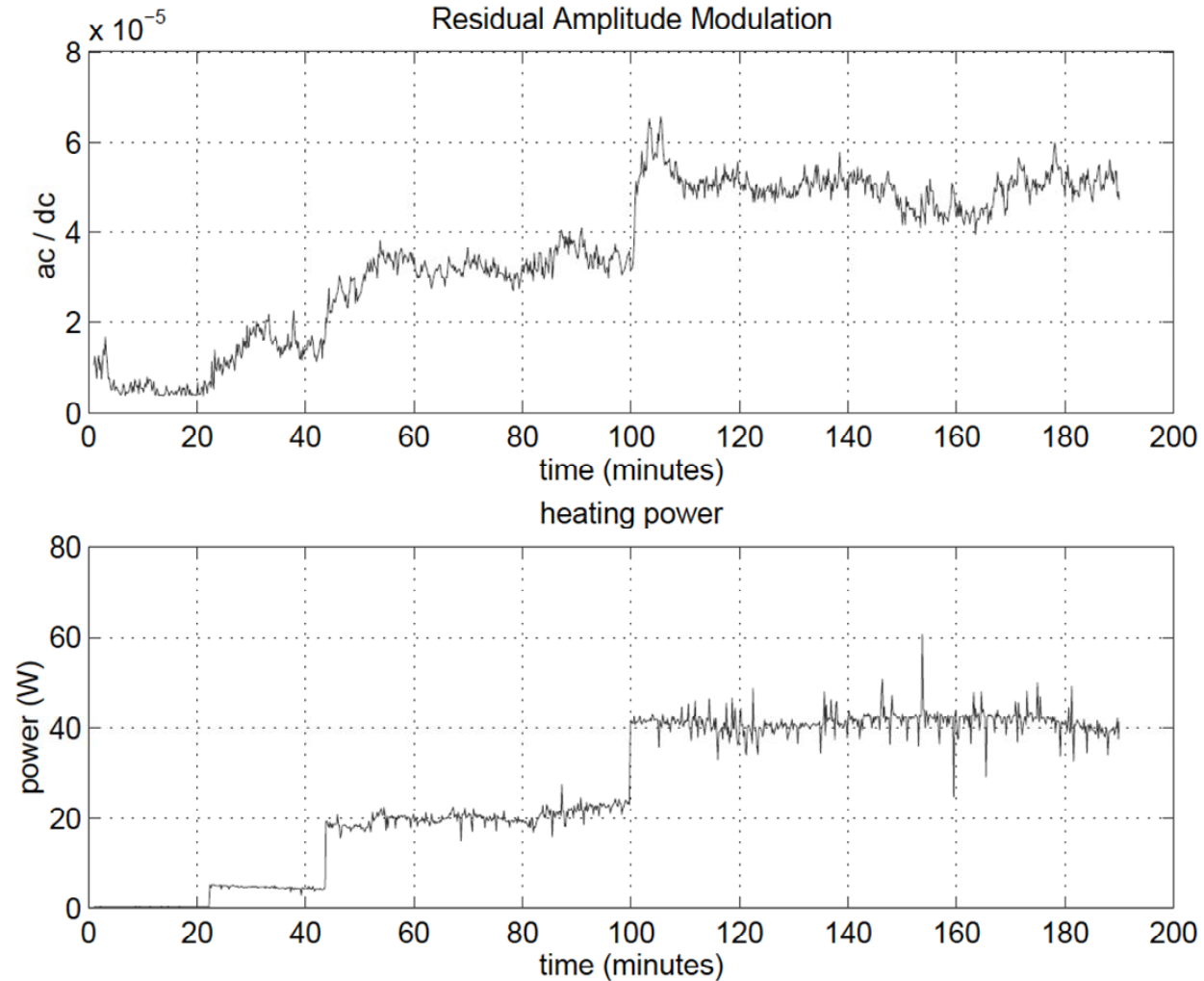


FIG. 4 – Measurement of RFAM induced by absorption/heating of the pump laser. The absolute change as the power is increased from 0 to 40 W is 5×10^{-5} , the RFAM swings at a given power level are $\sim 1 \times 10^{-5}$. This could be further reduced by applying temperature feedback to the housing.

With the heating beam off, the ratio of ac to dc powers is about 1×10^{-5} . That the RFAM is not zero is attributed to the alignment of the probe beam to the modulator axes. The fluctuations in the RFAM are at the 1×10^{-6} level. The measurement bandwidth was 300 Hz.

The main effect that one can see as the power is stepped up, correlated steps in the RFAM. This is clearly due to the fact that the increased power raises the temperature of the modulator and its housing. The change in temperature degrades the alignment of the modulator to the probe beam. If the modulator is realigned, the RFAM drops to the initial level. Because the heating laser is very

noisy, the fluctuations in the RFAM increase, but there are quiet times when the fluctuations are about the same as without the heating beam.

Further measurements are underway.

1.4.4 Damage

The intensity distribution in a Gaussian mode with total power P_o is:

$$P(r) = P_o \frac{2}{\pi} \frac{e^{-2\frac{r^2}{w^2}}}{w}$$

The intensity in the center is therefore:

$$P(r = 0) \approx 100 \frac{kW}{cm^2}$$

approximately 6000 times below the damage threshold quoted for 10 ns pulses. Although still to be verified, it seems unlikely that this power level will damage the coatings (or crystals). Raicol quotes a damage threshold for the uncoated RTP crystals of 1 GW/cm².

We have subjected an RTP crystal to 90 W of 1064 nm light for 300 hours, with no damage, induced absorption, or other changes noted. We have also destroyed a crystal instantly when the 90 W beam touched one of the electrodes.

1.5 Appendix: RTP properties, from <http://www.coretech.com.cn/RTP.htm>

Rubidium Titanyl Phosphate (RTiOPO₄ or RTP)

Applications and Advantages:

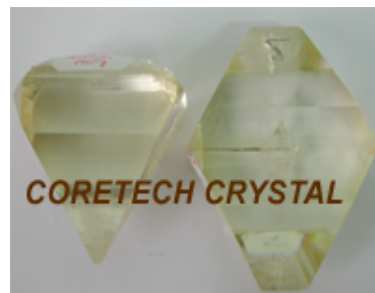
an excellent crystal for Electro Optical applications at high repetition rate.

High Damage Threshold, low Insertion Loss

not induce piezo-electric effect .

.Non-hygroscopic

High Extinction and Contrast Ratio



Standard specification:	
Dimension tolerance:	±0.1mm
Flatness:	<λ/8 @633nm
Surface quality: Scratch/Dig	10/5
Parallelism:	better than 30 arc sec.
Perpendicularity:	better than 30 arc min
Angle tolerance:	□θ < 0.5°, □φ < 0.5°

AR coating:	AR coatings
Clear aperture:	>90% central area
Transmitting wavefront distortion:	less than $\lambda/8$ @ 633nm

Physical and Chemical Properties:

Crystal Structure	Orthorhombic,
Lattice Parameters	$a = 12.96 \text{ \AA}, b = 10.56 \text{ \AA}, c = 6.49 \text{ \AA}$
Density	3.6 g/cm^3
Melting Point	$\sim 1000 \text{ }^\circ\text{C}$
Ferroelectric transition temperature	$\sim 810^\circ\text{C}$
Mohs Hardness	~ 5
Thermal Expansion Coefficients, $^\circ\text{C}$	$a_1=1.01 \times 10^{-5}, a_2=1.37 \times 10^{-5}, a_3=-4.17 \times 10^{-6}$
Hygroscopic Susceptibility	No
Dielectric Constant	$\epsilon_{\text{eff}} = 13.0,$
Color	Colorless
Ionic conductivity (room temperature, 10kHz)	10^{-8} S/cm

Optical properties:

Transmitting range:	350~4500 nm				
Sellmeier equations: $n_i^2=A_i+B_i[1-(C_i/\lambda)^2]-D_i\lambda^2$	index	A	B	C	D
	n_x	2.15559	0.93307	0.20994	0.01452
	n_y	2.38494	0.73603	0.23891	0.01583
	n_z	2.27723	1.11030	0.23454	0.01995
Absorption coefficient:	$< 0.0005 \text{ cm}^{-1} @ 1064 \text{ nm} < 0.04 \text{ cm}^{-1} @ 532 \text{ nm}$				

Nonlinear properties:

Nonlinear Coefficients:	$d_{15} = 2.0 \text{ pm/V}$
	$d_{24} = 3.6 \text{ pm/V}$
	$d_{31} = 2.0 \text{ pm/V}$
	$d_{32} = 3.6 \text{ pm/V}$
	$d_{33} = 8.3 \text{ pm/V}$
	$d_{\text{eff}} \text{ for type II SHG@}1064\text{nm} = 2.39 \text{ pm/V}$

Electro-optic coefficients:(pm/V)	Xcut Propagation Low frequency	Y cut Propagation Low frequency
	$r_{13} = 10.6$	
	$r_{23} = 12.5$	
	$r_{33} = 35$	$r_{33} = 38.5$
Static Half Wave Voltage @1064nm:	1445 V for a pair of 4x4x10mm	
	1,600 V for a pair of 4x4x20mm	
	1,700 V for a pair of 6x6x7mm	
	2,400 V for a pair of 6x6x20 mm	
Damage Threshold:10 nsec pulse	$> 600 \text{ MW/cm}^2 @ 1064 \text{ nm,}$	

2 Faraday Isolator

2.1 Proposed Faraday Isolator Design

2.1.1 Overview and conceptual design

The Faraday isolator (FI) design proposed for the LIGO upgrade³ is based on the design that will be used for Advanced LIGO. Figure 5 displays the schematic design of the FI. It consists of a Faraday rotator (FR) with two terbium gallium garnet (TGG) crystals and a quartz rotator (instead of a single TGG crystal as in conventional FRs), a $\lambda/2$ waveplate, a negative dn/dT material (deuterated potassium dihydrogen phosphate, KD_2PO_4 , or ‘DKDP’) for thermal lens compensation. In this design both thermally-induced polarization distortions and thermal focusing are reduced through the use of compensating elements. For depolarization compensation, the beam passes through two 22.5° TGG-based rotators and a reciprocal 67.5° quartz rotator placed in between them. In this configuration, the polarization distortions that the beam experiences while passing the first rotator (through the absorption of the beam and subsequent spatially-dependent birefringence) will be partially compensated in the second. For compensation of thermal focusing, absorption of laser light in the negative dn/dT material defocuses the beam and compensates the thermal focusing induced by absorption in the TGG. More details can be found in the papers by Khazanov, et al.^{4,5} and Mueller.⁶

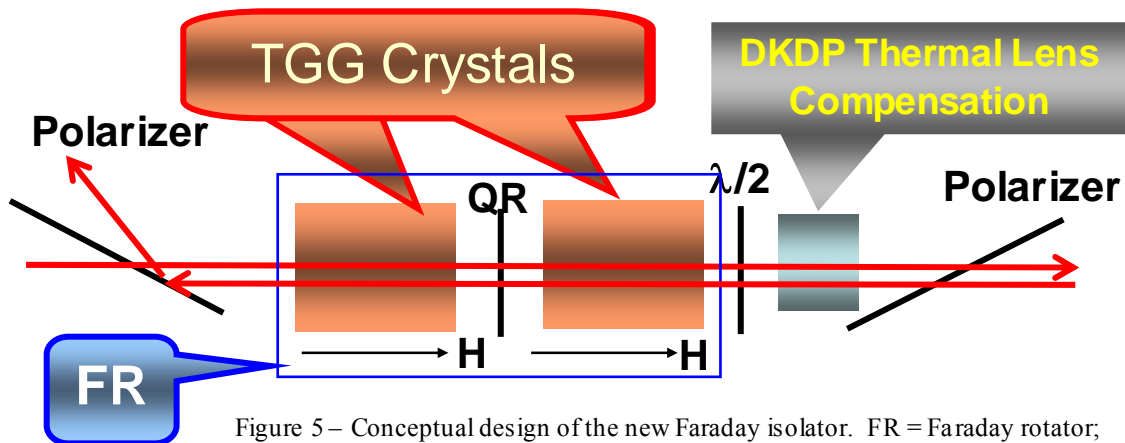


Figure 5 – Conceptual design of the new Faraday isolator. FR = Faraday rotator; TGG = terbium gallium garnet; QR = 67.5° quartz rotator; H = magnetic field; $\lambda/2$ = half waveplate.

³ LIGO-T050252-00-I, “Enhancements to the LIGO S5 Detectors”, P. Fritschel, R. Adhikari, and R. Weiss.

⁴ E. Khazanov, N. Andreev, A. Babin, A. Kiselev, O. Palashov, and D. H. Reitze, “Suppression of Self-Induced Depolarization of High-Power Laser Radiation in Glass-Based Faraday Isolators, J. Opt. Soc. Am B. **17**, 99-102 (2000).

⁵ E. Khazanov, N. Andreev, A. Mal’shakov, O. Palashov, A. Poteomkin, A. M. Sergeev, A. Shaykin, V. Zelenogorsky, Igor Ivanov, Rupal Amin, Guido Mueller, D. B. Tanner, and D. H. Reitze, “Compensation of thermally induced modal distortions in Faraday isolators”, IEEE J. Quant. Electron. **40**, 1500-1510 (2004).

⁶ G. Mueller, R. Amin, D. Guagliardo, Donavan McFeron, R. Lundock, D. H. Reitze, and D. B. Tanner, “Method for Compensation of Thermally-Induced Modal Distortions in the Input Optics Components of Gravitational Wave Interferometers”, Class. Quantum Grav. **19** 1793–1801 (2002).

2.1.2 Performance goals, design

To operate effectively at 30 W powers, we adopt the following performance goals for the new FI design:

Table 3 – Performance specifications for the new FI

<i>Parameter</i>	<i>Goal</i>	<i>Comment</i>
Optical throughput (%)	> 95%	Limited by absorption in TGG and DKDP, surface reflections in the FI components (total of 16 surfaces)
Isolation ratio (dB)	> 30 dB	Limited entirely by extinction ratio of thin film polarizers ⁷
Thermal lens power (m^{-1})	< 0.02	Leads to <2% reduction in mode-matching
Thermal beam drift (μrad)	< 100	Based on dynamic range of RBS actuators ⁸

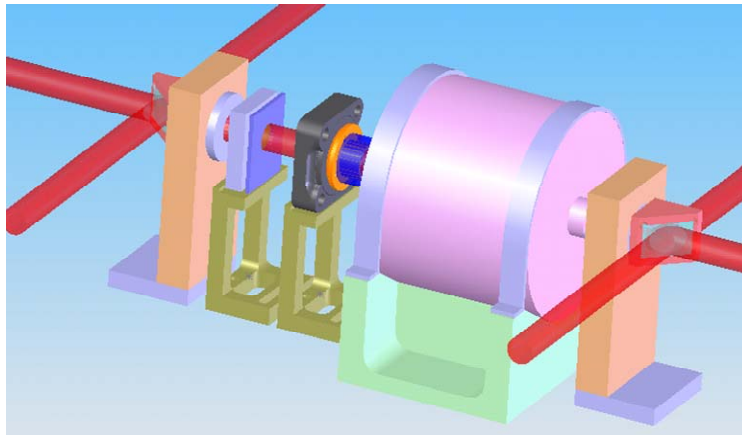


Fig. 6 – Schematic drawing of the FI, showing from front to back: i) 1/2 waveplate, ii) TPF, iii) FR, iv) 1/2 waveplate, v) DKDP, and vi) TPF. The breadboard and auxiliary mirrors are not shown. The separation distance of the initial 1/2 waveplate and TFPs depends upon the specific interferometer.

In addition, the FI must meet general requirements for in-vacuum materials set forth in LIGO-E960050-B-E “LIGO Vacuum Compatible Materials List”, D. Coyne. A complete list of requirements can be found in “Faraday Isolator Specifications for Advanced LIGO”⁹.

The physical layout of the FI is shown in Figure 6, and consists of the usual FI elements (polarizers, waveplate, FR) as well as the DKDP compensating element. The clear aperture of the system is 20 mm, the same as the FI currently in H2. The specific separation distance of the FI components depends upon the layout of the HAMs and differs for H1 (L1) and H2.

⁷ As we discuss below, it may be possible to use calcite wedge polarizers (which have extinction ratios in excess of 10^5), which would improve the isolation specification to > 40 dB.

⁸ Ken Franzen and Valera Frolov, personal communication

⁹ LIGO-T050226-00-D, “Faraday Isolator Specifications for Advanced LIGO”, D.H. Reitze, et al.

The two-crystal design of the FR mandates a larger housing and magnetic field. This has consequences for the in-vacuum layouts. The large housing eclipses the laser beam in H1 and L1. The FI must be moved from its current position between SM1 and MMT1 to a position in between MMT1 and MMT2 (but still in HAM1), and SM1 will need to be repositioned. In addition, the ‘acceptance angle’ of the FI (defined by the isolation ratio sensitivity to input angle) is reduced relative to the current FIs. For H2, it may be possible to leave the FI in its current location between SM1 and SM2, at a reduced isolation ratio. These changes are described in more detail below.

2.1.3 Size and weight

The FR housing is 15.5 cm in diameter by 16.1 cm long. The FR weighs 30.8 lbs (37 lbs with stand). The total FI assembly will add approximately 40 lbs to HAM1 (H1, L1) and 30 lbs to HAM7 (H2)¹⁰ and require the removal and repositioning of some counterweights.

2.1.4 Choice of polarizers

The performance of the FI depends on the type of polarizer used; both calcite wedges and TFPs have been tested. Both offer advantages and disadvantages which we summarize here.

2.1.4.1 Calcite wedges

Calcite wedge polarizers use the natural birefringence of calcite to separate orthogonal polarizations. The polarizers used in these experiments were low absorption 2.5 mm thick polarizers with a 4.3° wedge angle. They were obtained from the IAP.

2.1.4.1.1 Advantages of calcite wedge polarizers

- Calcite polarizers possess very high extinction ratios ($>10^5$), and thus provide for the optimal isolation performance. The isolation data presented below was obtained using calcite polarizers.
- Calcite polarizers offer higher overall transmission than TFPs (~ 97% vs 93% for TFPs)

2.1.4.1.2 Disadvantages of calcite wedge polarizers

- Because the calcite polarizers rely on the (small) difference in the ordinary and extraordinary index of refraction, the exit angle of the ordinary and extraordinary rays is quite small, on the order of 10 mrad. In order to separate the REFL beam from the incident beam, a propagation distance of at least 1 m is required before the pickoff mirror can be placed. This in turn requires that the REFL beam reflect off both the MMT1 and the SM (H1, L1) or SM1 (H2) before pickoff.
- The thermal drift of the calcite polarizers as the loading power is increased is a factor of 20 worse than TFPs, but still within the 100 μ rad limit.
- The wedge introduces an angular displacement of the beam, requiring a small change in the layout. We do not believe that this is a significant disadvantage.

¹⁰ The H2 FI was replaced in 2003; the H2 FI assembly weighs more than the older H1 and L1 FIs.

2.1.4.2 Thin film polarizers

The TFPs used in these experiments were obtained from CVI and LZH. Most of the experiments were done with CVI polarizers.

2.1.4.2.1 Advantages of TFPs

- The thermal steering of the TFPs is negligible at powers up to 30 W.
- The rejected REFL beam comes off of the polarizer at 45°, making it easy to direct the beam to the ISC table periscope

2.1.4.2.2 Disadvantages of TFPs

- The extinction ratio of the TFPs is ~ 1000 . This places an upper limit of the FI isolation ratio of 30 dB.
- The transmission of the TFPs is lower than that of the calcite wedges.

2.2 Measured Optical Performance

We have performed a series of measurements of the proposed FI design, including optical isolation, thermal lensing, optical throughput, and thermal beam drift.

2.2.1 Thermal birefringence and optical isolation

Optical isolation was measured using the ratio of the power transmitted through the first polarizer to reflected power from the HR mirror: optical isolation in dB = $10 \log(P_{in, backward}/P_{T, backward})$. For these measurements, high quality calcite wedge polarizers (extinction ratio $> 10^5$) to be limited by the thermal depolarization rather than the extinction ratio of the polarizers.

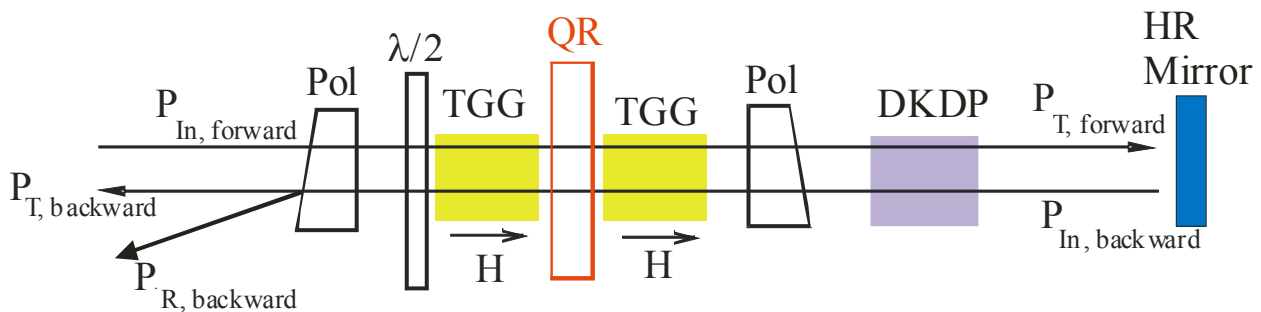


Fig. 7 – Measurement of isolation ratio for new FI design. The polarizers (Pol) are high quality calcite wedges with extinction ratios $> 10^5$. The isolation ratio is measured as $10\log(P_{T, backwards}/P_{In, backwards})$

Figure 8 shows the measured isolation ratio as a function of single pass power for both the new design and the original LIGO 1 EOT FI design. At 30 W, we obtain ~ 46 dB isolation. If TFPs are used, the expected isolation ratio would decrease to ~ 30 dB.

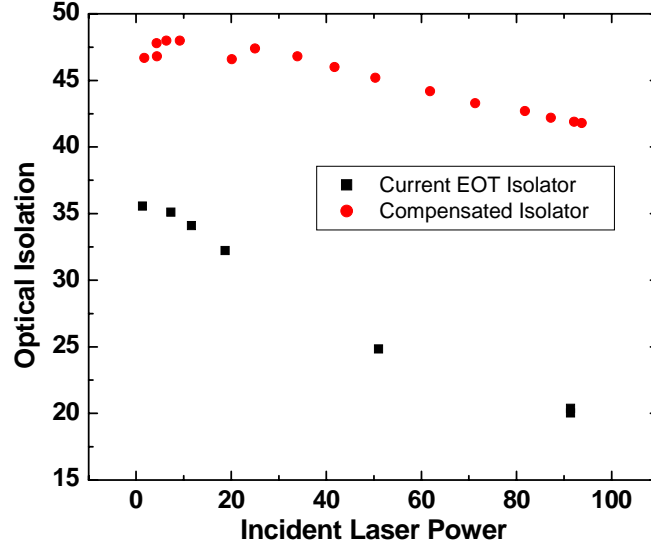


Fig. 8 – Measured isolation ratio as function of incident laser power for the proposed design (red circles) and current LIGO 1 FI (black squares).

Because the quartz rotator in the FR is birefringent and oriented such that the optical axis is parallel to the laser propagation, the isolation ratio depends sensitively on the angle that the propagating beam makes with the optical axis of the FR. Slight angular deviations of the propagation axis of the laser w.r.t. the quartz optical axis produce linear birefringence whose magnitude depends upon the relative deviation angle of the beam with respect to the polarization axis of the beam. The worst case occurs for deviations 45° w.r.t to the polarization axis. For this case, the measured sensitivity to angle is shown in Fig. 9. The isolation falls off steeply for incident angles greater than $\pm 0.25^\circ$ (± 4.4 mrad). The acceptance angle of the FI is determined by the apertures of the mirrors bracketing the FI and their separation distance. For H1 and L1, the FI will be placed downstream of MMT1 (in between MMT1 and MMT2); this defines an acceptance angle $\theta_{4k} = \pm (\text{aperture of MMT2})/(\text{distance from FI to MMT2}) \sim 0.0375/15 = \pm 2.5$ mrad. For H2, the FI will be placed in between SM1 and SM2, corresponding to an acceptance angle $\theta_{2k} = \pm 32$ mrad. For alignments in which the H2 beam is substantially displaced from the centers of SM1 and SM2, reductions in isolation to below 30 dB may result. Thus, it may be prudent to reposition the FI to downstream of the MMT1 in H2.

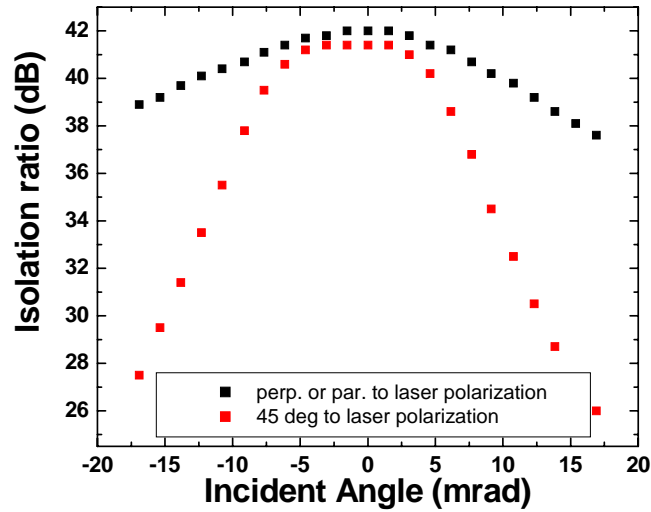


Fig. 9 – Isolation ratio as a function of incident angle w.r.t the optical axis of the FR. Black points correspond to angular deviations parallel or perpendicular to the laser polarization axis and represent the minimum depolarization. Red points correspond to angular deviations at 45° to the polarization axis and represent the worst case.

2.2.2 Thermal lensing

Thermal lensing was determined by measuring the beam divergence as a function of incident laser power for i) the FI alone (without the DKDP), ii) the DKDP alone, and iii) the entire thermally compensated FI.

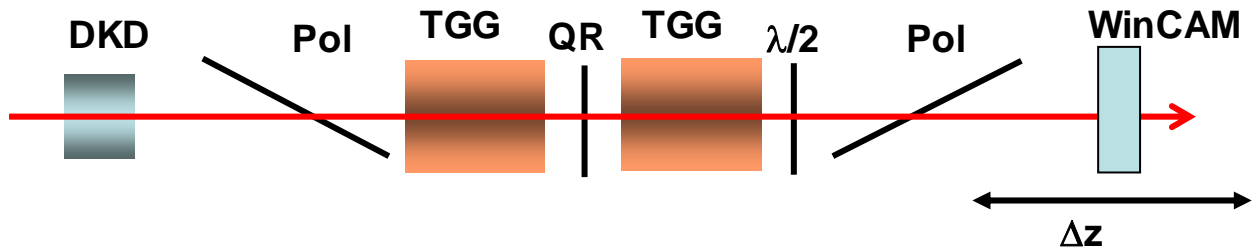


Fig. 10 – Measurement of the thermal lensing in the FI. In this case, the DKDP was placed before the FI and only the single pass lensing was measured. However, the location of the DKDP in the upgrade will either be in between the polarizers or between the FI and the PRM

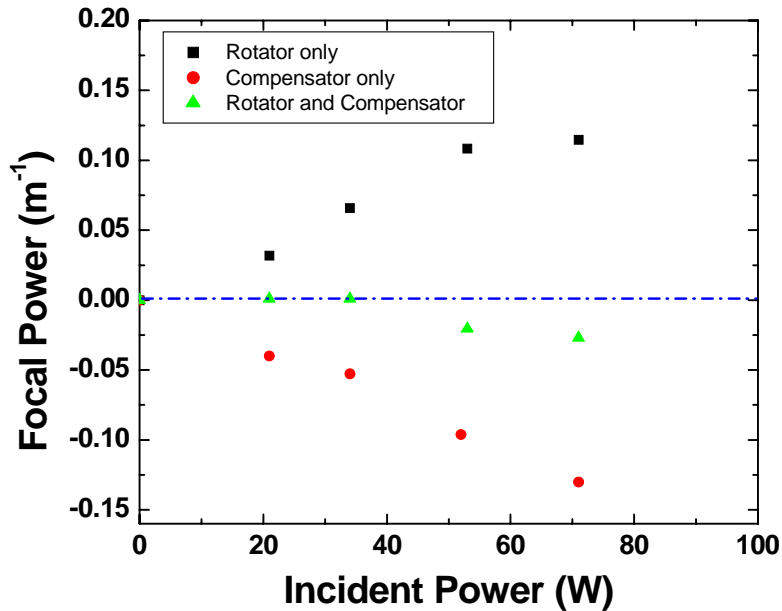


Fig. 11 – Thermal focal power of the FI as a function of incident laser power. The black squares show the focal power (in m^{-1}) for the FI without thermal compensation. The red circles display the measured focal power of the DKDP. The green triangles display the measured focal power for the fully compensated FI.

Figure 11 displays the thermal lensing induced in the FI as function of single pass power. For these measurements, there was no backward propagation. The total thermal lensing (green triangles) at 30 W of incident power is negligible; at 70 W, a focal power of approximately 0.025 m^{-1} (corresponding to a thermal focal length $f = 40 \text{ m}$). The magnitude of thermal compensation depends on the absorption coefficient and the length of the DKDP crystal. It is difficult to control the absolute absorption in DKDP since it depends sensitively on the stoichiometry of deuterium. For these measurements, it was known in advance from absorption measurements that the DKDP would overcompensate for the thermal lens in the FR. Better results can be obtained by further thinning of the DKDP crystal; the DKDP will be optimized for the FIs used in the LIGO upgrade.

2.2.3 Thermally induced beam steering

The measurement set-up for determining the thermally-induced tilt as the power is increased is shown in Fig. 12. Measurements were made for an incident power of 30 W; zero time corresponds to the time at which power was sent into the FI. These measurements were performed without the DKDP crystal.

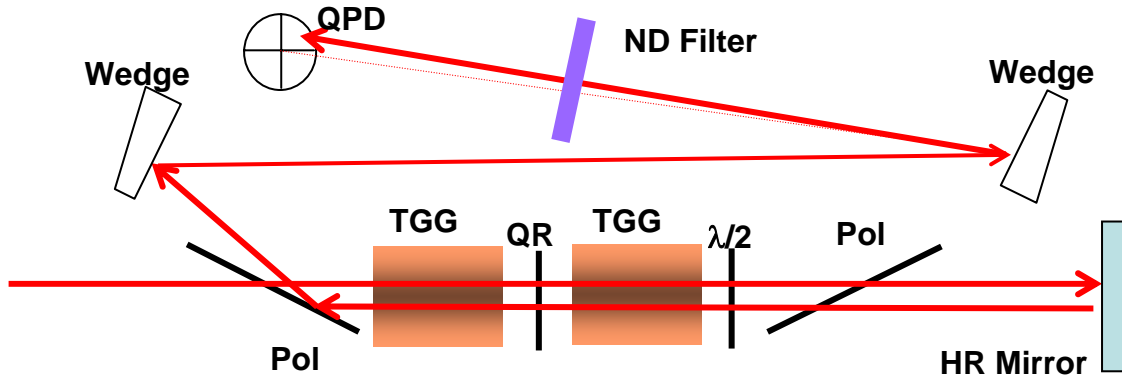


Fig. 12 – Experimental set-up for measuring power-dependent thermal steering.

2.2.3.1 Calcite polarizers

The thermal drift with calcite wedges as polarizers for 30 W incident power is shown in Fig 13. Measurements at lower powers show that the magnitude of the drift is linear in power. Thus, a thermal drift coefficient of $1.3 \mu\text{rad}/\text{W}$ is inferred. The vertical and horizontal drifts are comparable in magnitude; the origin of the vertical drift is unknown at this time.

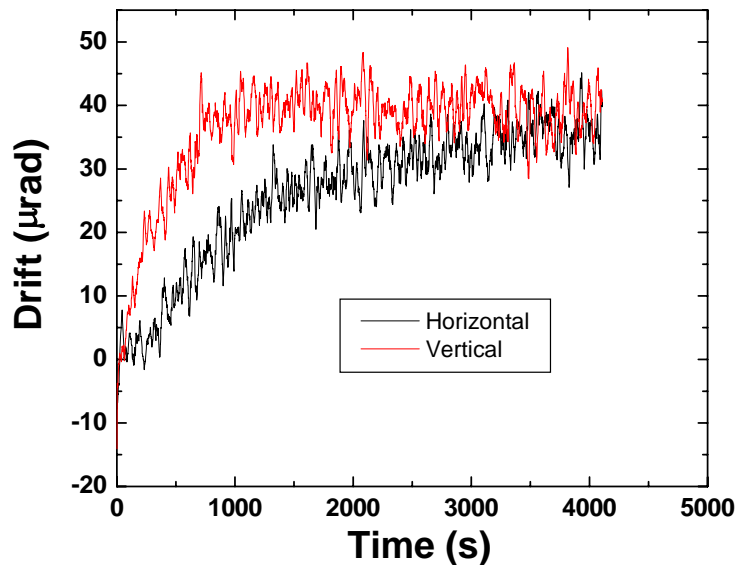


Fig. 13 – Change in angle of the rejected FI beam versus time for calcite polarizers from a cold start (no power) to 30 W.

2.2.3.2 Fused Silica Thin Film Polarizers

Thermal drift using TPFs with 30 W incident power is shown in Fig 14, corresponding to a thermal drift coefficient of $130 \text{ nrad}/\text{W}$. The vertical drift is slightly larger than the horizontal drift, but both are quite small when compared to the calcite wedges.

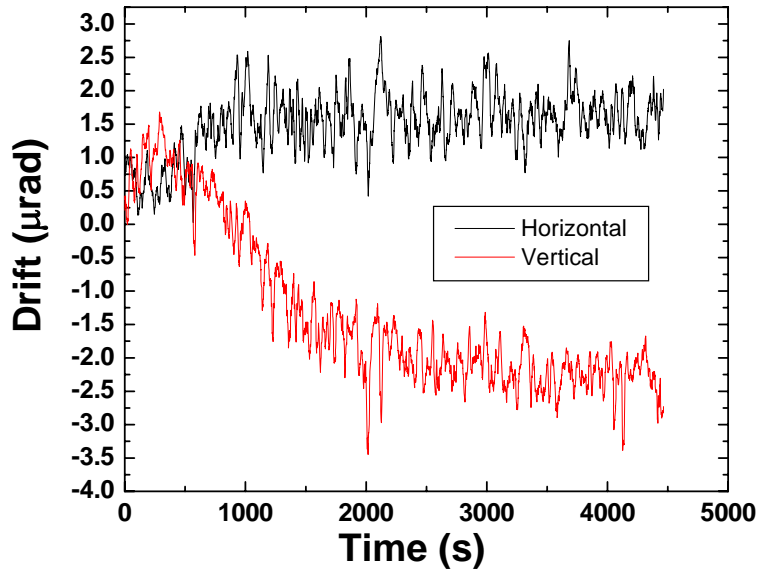


Fig. 14 – Change in angle of the rejected FI beam versus time for TFPs from a cold start (no power) to 30 W.

2.2.4 Optical throughput

The optical throughput was measured for the full FI using both calcite and wedge polarizers. The fractional transmitted and rejected light are as follows:

- FI with TFPs:
 - Percent transmitted: $93.3\% \pm 0.3\%$
 - Percent rejected: $90.3\% \pm 0.3\%$ (defined as $P_{r, backward}/P_{in, backward}$, where $P_{in, backward}$ is the light power incident on the FI in the reverse direction and $P_{r, backward}$ is the rejected light power)
- FI with calcite wedge polarizers:
 - Percent transmitted: $98.3\% \pm 0.3\%$
 - Percent rejected: $94.6\% \pm 1.0\%$

2.3 Modifications to the current in-vacuum optical layout

2.3.1 4K IFO

Figures 15 and 16 show the new layout for the repositioned FI for the 4km IFOs. In addition to repositioning of the FI, other changes to be made include:

- a) In order to accommodate the large size of the FR housing, both SM1 and MMT1 will need to be moved from their current location towards the edge of HAM1. SM1 will be shifted $\sim xx$ cm along the MC beam propagation direction, and MMT1 will need to be shifted approximately xx cm toward the edge of the table. In addition, the angle of incidence of the beam on MMT1 will increase from 4.9° to 10.8° .

- b) The half waveplate currently located between MC3 and SM1 which rotates the polarization from 's' to 'p', will be moved to after SM1. This will decrease the transmission of the SM 1 from $\sim 2\%$ to $\sim 0.2\%$. In addition, the reflectivity of SM1 depends on the angle of incidence, which will further decrease the transmission. The total transmitted power of SM1 for 30 W incident is expected to somewhere in the range 30-60 mW, be we need to measure it to be sure.
- c) The transmitted SM1 beam used to PSL intensity stabilization will be re-routed to avoid the new FI. This will require the addition of two fixed kinematic mounts and mirrors
- d) The breadboard of the FI (not shown in the drawings) assembly will be wedged to account for the beam rise from MMT1 to MMT2. (HAM 2 is lower than HAM 1 so the global coordinate axes slope downwards at both sites. The slopes are different, so site-specific breadboards are required.)
- e) Beams dumps will be moved to their new appropriate positions.

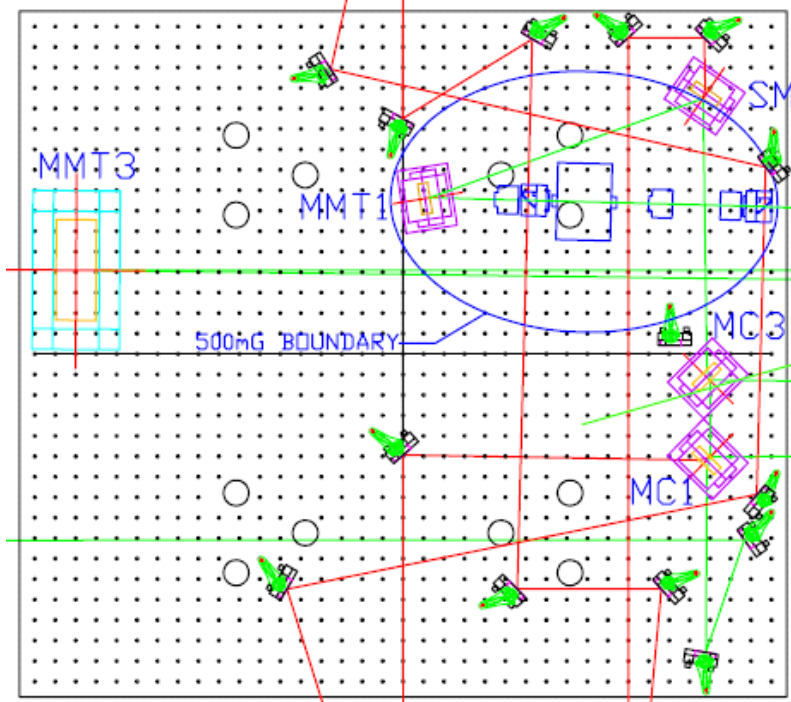


Figure 15 – Proposed optical layout for 4K HAM 1. Clamps for the fixed mirrors will be moved to the appropriate location for tie down. The FR housing does not clip the beam from MMT3 to the PRM since their elevations are different.

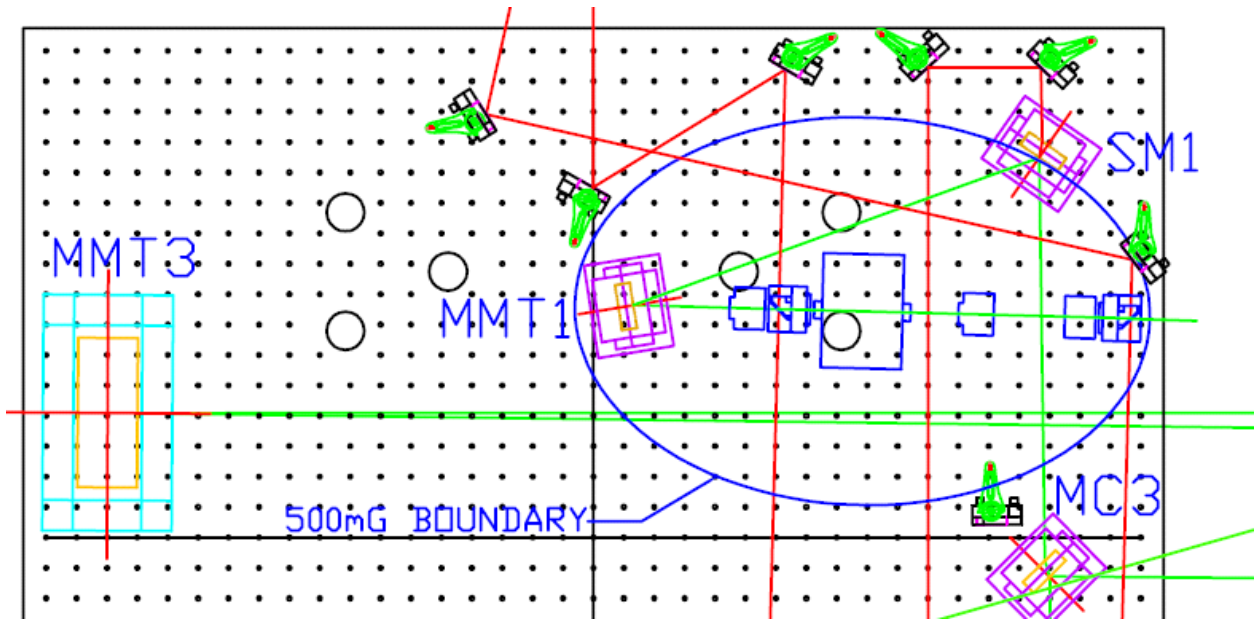


Figure 16 – Close-up of 4K Faraday isolator location.

2.3.2 2K IFO layout

Figure 17 shows the new layout for the 2k IFO. This replacement is relatively simple. Only the transmitted SM1 beams and reflected RM beam lines will need to be moved.

Should the isolation ratio dependence on angular alignment through the FI prove to be a problem, it is possible to move the FI downstream of MMT1, although getting all of the ancillary diagnostic beams (not including REFL) may require complicated paths.

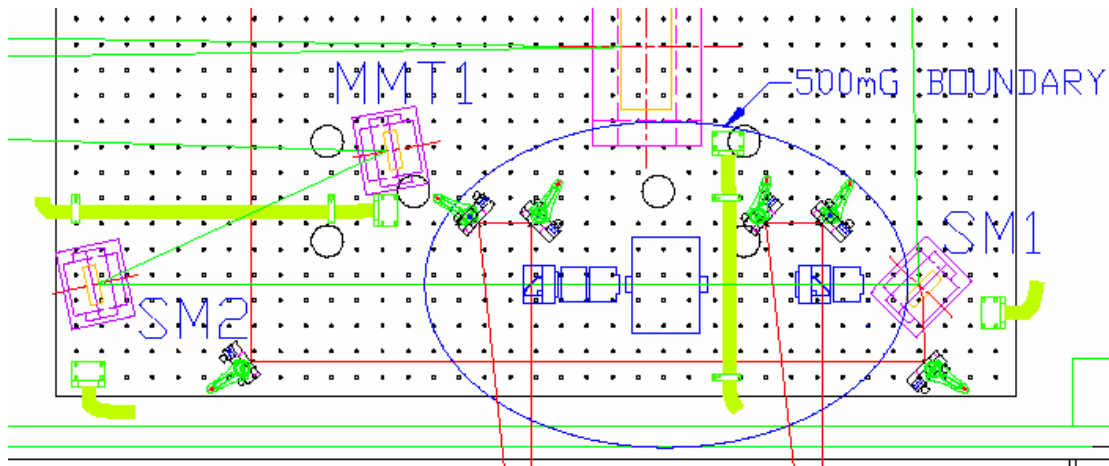


Figure 17 – Proposed optical layout for 2K HAM 7.

2.4 Magnetic field coupling to IO suspended mirrors

The FR dual crystal design uses a more complicated magnetic field configuration to achieve uniform fields in the TGG crystals. The maximum magnetic field is 1.5 T; this is slightly more than the 20 mm aperture Electro-optics Technology FI currently in use in H2. The magnets are composed of sintered Nd:Fe:B, as are the LIGO FI magnets.

A measurement of the magnetic fields and an analysis of the coupling of the Advanced LIGO FI to the mode cleaner mirrors have been performed for Advanced LIGO based on the requirement that the fields do not induce frequency noise above that required by Advanced LIGO.¹¹

The requirements derived for the maximum magnetic field gradient to induce a dynamic force on the mode cleaner mirrors are:

$$\nabla^2 B_{\parallel\mu}^{max} \leq 1.35 \times 10^6 \left(\frac{f}{10\text{Hz}} \right)^{3/2} \left(\frac{3.89\text{kg}}{m} \right) \frac{\text{Gauss}}{m^2} \quad (1)$$

where $B_{\parallel\mu}$ is the component of field oriented parallel to the magnetic dipole on the mirror and m is the mass of the mirror. The requirements derived for the maximum magnetic field gradient to

¹¹ “Analysis of Stray Magnetic Fields from the Advanced LIGO Faraday Isolator”, T060025-00-D, G. Mueller, et al

induce a dynamic torque on the mode cleaner mirrors (which couples with an off-centered beam to induce a length change) are:

$$\frac{\partial B_{\perp\mu}^{max}}{\partial r} \leq 3 \times 10^6 \left(\frac{f}{1 \text{ Hz}} \right)^{3/2} \left(\frac{8.3 \times 10^{-3} \text{ kg m}^2}{I} \right) \left(\frac{\mu}{0.0107 \text{ A m}^2} \right) \frac{\text{Gauss}}{\text{m}^2} \quad (2)$$

where $B_{\perp\mu}$ is the component of the magnetic field perpendicular to the dipole moment μ of the mirror magnet and I is the moment of the inertia of the mirror.

These requirements were derived assuming stack motions of the Advanced LIGO seismic isolation platforms. Using the measured ground motion at LLO, transfer functions of the current HAM stacks, and $m = 0.25 \text{ kg}$ and $I = 1 \times 10^{-4} \text{ kg m}^2$ for the current small optics mirror, the same analysis yield requirements for the upgrade. At 100 Hz, we find that:

$$\nabla^2 B_{\parallel\mu}^{max} \leq 1.35 \times 10^{11} \frac{\text{Gauss}}{\text{m}^2} \quad \frac{\partial B_{\perp\mu}^{max}}{\partial r} \leq 3 \times 10^8 \frac{\text{Gauss}}{\text{m}^2}$$

The measured fields and computed gradients are shown in Figure 18. The gradients are well below the required values for distances greater 5 cm and orders of magnitude below for all suspended optics in the layouts shown above.

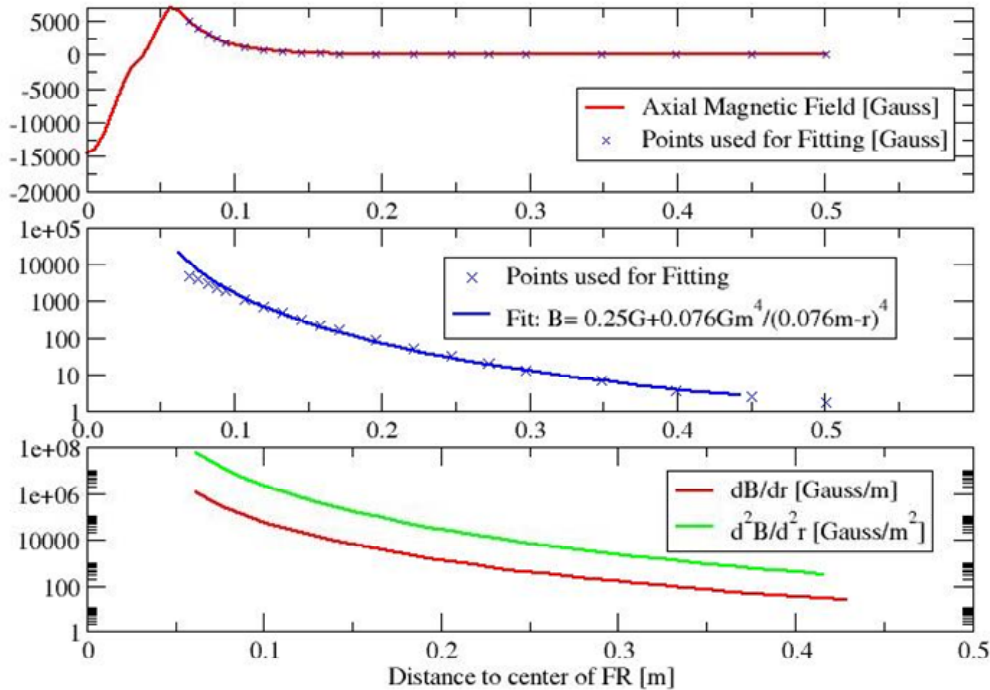


Fig. 18 – Measured axial magnetic fields and computed field gradients based on fitting the axial field.

2.5 Vacuum compatibility

The prototype IAP FR was not designed or assembled with LIGO vacuum requirements in mind, and it has not yet been certified for in-vacuum operation. Some parts of the FR housing will need to be replaced (brass, e.g.) before undergoing baking, although it will be impossible to completely disassemble the housing and magnets for cleaning, since the orientation of the magnets in the housing results in a strong repulsive force of the individual solenoids.

Our plan is to try a clean and bake on the FR in the next month (either at LHO or CIT) and see how it fairs. Should it fail, we will institute clean assembly procedures (components are first clean and baked and then assembled according to LIGO spec) for the new FIs.

2.6 Assembly, Alignment, and Vacuum Incursion Plan

1. Upon receipt, all components will be baked and checked for vacuum compliance according to LIGO Vacuum Protocols
2. After baking, components will be assembled, aligned, and characterized in the LLO/LHO clean optics lab. This includes:
 - a. Assembly and testing of the polarizers after baking
 - b. Assembly and testing of the FR after baking
 - c. Build-up and alignment of the FI assembly

- d. Measurement of optical throughput, isolation ratio, polarization purity, and if possible, thermal defocusing, depolarization and associated time constants.
3. Completed FI assembly will be prepped for transport to the LVEA.
4. Vacuum installation plan – TBD depending other planned activities.

3 Costs

3.1 Electro-optic Modulator

The itemized cost per EOM is as follows:

<i>Item</i>	<i>Vendor</i>	<i>Quantity</i>	<i>Unit Cost</i>	<i>Total Cost</i>
RTP crystals	Raicol	1	\$2600	\$2600
Machined Components	UF	1	\$400	\$400
Electronics	UF	1	\$100	\$100
Shipping				\$20
TOTAL				\$3120

3.2 Faraday Isolator

The itemized cost per FI is as follows:

<i>Item</i>	<i>Vendor</i>	<i>Quantity</i>	<i>Unit Cost</i>	<i>Total Cost</i>
20 mm Faraday rotator	IAP	1	\$10000	\$10000
Half waveplates	CVI Laser	1	\$530	\$530
TFPs	LZH	2	\$1000	\$2000
(Calcite polarizers	IAP	2	\$1000	\$2000)
DKDP compensation plate	IAP	1	\$1000	\$1000
UHV pedestals and clamps	New Focus, Inc.	4	\$28	\$112
UHV Rotation Stages	CVI Laser	3	\$149	\$447
UHV Faraday rotator pedestal	UF	1	\$20	\$20
UHV Breadboard	UF	1	\$50	\$50
UHV polarizer adaptors	UF	2	\$30	\$60
2" diameter fixed mirror mount	UF	1	\$30	\$30
Shipping				\$200
TOTAL				\$14449

We assume that there will be a sufficient number of spare DLC mounts available in the optics labs for re-routing the MC transmitted beam. If not, either DLC mounts can be ordered at additional cost, or fixed mounts can be used. Also, some spare 2" supermirrors will be needed.